PNAS RESEARCH ARTICLE | EARTH, ATMOSPHERIC, AND PLANETARY SCIENCES

A transient peak in marine sulfate after the 635-Ma snowball Earth

Yongbo Peng[a,b], Huiming Bao[a,b,1], Ganqing Jiang[c], Peter Crockford[d,e], Dong Feng[f], Shuhai Xiao[g], Alan Jay Kaufman[h], and Jiasheng Wang[i,j]

Edited by Mark Thiemens, University of California San Diego, La Jolla, CA; received September 20, 2021; accepted March 24, 2022

A series of dramatic oceanic and atmospheric events occurred in the immediate aftermath of the Marinoan "snowball Earth" meltdown ~635 My ago. However, at the 10- to 100-ky timescale, the order, rate, duration, and causal-feedback relationships of these individual events remain nebulous. Nonetheless, rapid swings in regional marine sulfate concentrations are predicted to have occurred in the aftermath of a snowball Earth, due to the nonlinear responses of its two major controlling fluxes: oxidative weathering on the continents and pyrite burial in marine sediments. Here, through the application of multiple isotope systems on various carbon and sulfur compounds, we determined extremely ^{13}C-depleted calcite cements in the basal Ediacaran in South China to be the result of microbial sulfate reduction coupled to anaerobic oxidation of methane, which indicates an interval of high sulfate concentrations in some part of the postmeltdown ocean. Regional chemostratigraphy places the ^{13}C-depleted cements at the equivalent of the earliest Ediacaran ^{17}O-depletion episode, thus confining the timing of this peak in sulfate concentrations within ~50 ky since the onset of the deglaciation. The dearth of similarly ^{13}C-depleted cements in other Proterozoic successions implies that the earliest Ediacaran peak in marine sulfate concentration is a regional and likely transient event.

snowball Earth | oxidation | sulfate | ^{17}O anomaly | methane oxidation

Significance

Earth system's response to major perturbations is of paramount interest. On the basis of multiple isotope compositions for pyrite, carbonate-associated sulfate, carbonates, and organics within, we inferred that the much-debated, enigmatic, extremely ^{13}C-depleted calcite cements in the ~635-Ma cap carbonates in South China preserve geochemical evidence for marine microbial sulfate reduction coupled to anaerobic oxidation of methane. This interpretation implies the existence of a brief interval of modern-level marine sulfate. We determined that this interval coincides with the earliest Ediacaran ^{17}O-depletion episode, and both likely occurred within ~50 ky since the onset of the 635-Ma meltdown, revealing an astonishing pace of transformation of the Earth system in the aftermath of Earth's latest snowball glaciation.

Uncovering how the lithosphere, hydrosphere, atmosphere, and biosphere respond to massive disruptions in the past is of paramount importance in understanding the Earth system and its evolution. Perhaps no case is more salient than postglaciation responses after the termination of snowball Earth intervals. Recently, a consistent postglacial sequence of events has emerged for Earth's latest panglaciation, the Marinoan snowball Earth event (ca. 635 Ma), through multiple independent lines of evidence. What has come to light is that within a relatively short period of time from the onset of deglaciation, the Earth system went through 1) a large increase to continental weathering rates (1–3); 2) widespread porewater deposition of pyrite (4); 3) a rapid rise of seawater pH (5); 4) a surge of primary productivity (6); 5) the global deposition of cap carbonates (7); 6) the global deposition of barite crystal fans (8–10); and 7) the destratification of a meltwater lid with deep saline seawater (11, 12). These events were very likely accompanied by a rapid drawdown of atmospheric CO_2 and a rapid rise of atmospheric O_2 (2, 13), resulting in the earliest Ediacaran ^{17}O depletion (previously named the Marinoan ^{17}O depletion) episode recorded within sulfate in cap carbonate sequences worldwide (14–18). This "aftermath" sequence of events was then followed by pulsed surface oxidation as well as the diversification and extinction of acritarchs in South China (19, 20). Testing the validity of this sequence of events requires the examination of event order, the quantification of pertinent rates, and the deconvolution of causal-feedback relationships. The sequence presented above also portends what events were likely to follow. One such prediction across this sequence is large, regional fluctuations in marine sulfate concentrations ($[SO_4]$) in the earliest Ediacaran period, due to nonlinear responses in sulfate fluxes.

Like all chemical components of seawater, $[SO_4]$ is determined by source and sink fluxes. At 10- to 100-ky time scales (21, 22), source fluxes include oxidative weathering of sulfides on land; evaporite dissolution; and the oxidation of volcanic and biogenic sulfur gases that are delivered to the oceans through rivers, subterranean groundwater discharge, and the atmosphere. An oxic/anoxic interface in seawater or sediment columns can also be a place where sulfate is added back to seawater via the oxidation of H_2S produced by microbial sulfate reduction (MSR). Quantitatively significant sink fluxes include pyrite burial, expansion of marine H_2S reservoir, and evaporite deposition. Considering the lack of evidence for any major changes in volcanic activities, evaporite weathering, or evaporite deposition in South China during the early Ediacaran period, we argue that the volcanic and evaporite fluxes were not major drivers in perturbation of the sulfur cycle. The dominant controls of marine $[SO_4]$ are, therefore,

Author contributions: Y.P. and H.B. designed research; Y.P., H.B., P.C., and D.F. performed research; Y.P., G.J., P.C., D.F., S.X., A.J.K., and J.W. contributed new reagents/analytic tools; Y.P., H.B., G.J., P.C., and S.X. analyzed data; and Y.P., H.B., and P.C. wrote the paper.

The authors declare no competing interest.

This article is a PNAS Direct Submission.

[1]To whom correspondence may be addressed. Email: bao@nju.edu.cn.

This article contains supporting information online at http://www.pnas.org/lookup/suppl/doi:10.1073/pnas.2117341119/-/DCSupplemental.

Published May 2, 2022.

oxidative weathering on the continent, pyrite burial in marine sediments, and the expansion or contraction of the marine H_2S reservoir.

Experimental studies infer that pyrite oxidation follows a half-order reaction rate law with respect to a large range of pO_2 (23), where increases in pO_2 lead to increases in pyrite oxidation rates. Pyrite oxidation is also a surface reaction, and the accessible surface area is predicted to be the highest at the beginning of the Marinoan meltdown because of the enormous amount of glacial rock flour and loess (24). Therefore, it is likely that at the onset of deglaciation, the sulfate flux from oxidative weathering would have risen rapidly, until the combination of atmospheric conditions and the exhaustion of rock flour returned the flux to a similar or higher Proterozoic background value.

For the pyrite burial flux and the size of the H_2S reservoir, one has to consider primary productivity (i.e., availability of organic matter), pO_2, sedimentation rate, Fe availability, and shelf area (i.e., sea level). A surge in primary productivity is expected at the very beginning of deglaciation due to high nutrient fluxes from the continents through intense continental weathering (25). A high rate of organic matter burial would facilitate overall Earth surface oxidation and, in the meantime, may result in an imbalance between fluxes of sulfate reduction and sulfide oxidation. Such an imbalance could lead to an enhanced pyrite burial, as evident from the massive pyrite deposition in the topmost Nantuo (NT) diamictites, which represent Marinoan glacial deposits in South China (4). Thus, it is predicted that at the onset of meltdown, most sulfate was rapidly reduced to sulfide and buried as pyrite, given sufficient Fe supply. However, after the meltdown, nutrient and sediment supplies would decrease, eustatic sea level would rise (but relative sea-level change would be highly heterogeneous depending on location due to isostatic adjustment), atmospheric pCO_2 would fall, and atmospheric pO_2 would rise over time (16). Importantly, the tempo of these events would vary substantially as the Earth's surface returned to a stable state. Such variability would have rendered the evolving fluxes of oxidative weathering products and pyrite burial (including fluctuations of the H_2S reservoir) asynchronous in time, heterogenous in space, and variable in magnitude. As such, at near-shore sites, short-term and high-amplitude swings of marine $[SO_4]$ are speculated to have occurred in the earliest Ediacaran oceans.

Testing predictions of the postglacial sulfur cycle requires that one measures marine $[SO_4]$ at the 10- to 50-ky level of resolution in order to correlate with the events outlined above. Modeling $[SO_4]$ changes is one approach to reconstruct the trajectory of the postglacial sulfur cycle; however, a large number of unknowns and a lack of constraints on key parameters render such inferences limited. Qualitatively, the presence of sulfate at the onset of the Marinoan meltdown is evident from the widespread occurrence of porewater pyrite deposition on top of Marinoan diamictites (4). A highly variable and, therefore, small initial sulfate pool is inferred from the highly variable $\delta^{34}S$ values for the barite crystal fans in the cap carbonate sequences (8, 17). However, additional evidence is needed to corroborate these findings with respect to the evolution of the earliest Ediacaran sulfate reservoir.

The sporadic occurrence of extremely ^{13}C-depleted ($\delta^{13}C$ lower than –30‰) calcite cements (termed "^{13}C-depleted cements" forward) in basal Ediacaran cap carbonates potentially provides such evidence. Lithologically, the dark-colored, ^{13}C-depleted cements occur as generations of cement in voids, cavities, and crusts on breccias or as thin lenses that are parallel to the bedding of the cap dolostones that overlies the NT diamictites and underlies Member II shales of the Doushantuo Formation (26–29). If, indeed, the ^{13}C-depleted cements were deposited from seawater via MSR coupled to anaerobic oxidation of methane (AOM) (30), they could in principle offer a quantitative constraint on marine $[SO_4]$ because their precipitation requires a large proportion of dissolved inorganic carbon (DIC) to be sourced from AOM and thus requires a high concentration of sulfate in water even in a closed system (31). However, the origin of the basal Ediacaran ^{13}C-depleted cements remains contested. The ^{13}C-depleted cements were initially proposed to have precipitated early diagenetically, based on carbonate $\delta^{13}C$ data (30), but were reinterpreted to have formed from hydrothermal fluids on the basis of carbonate clumped isotope thermometry and a thermal history implied by coexisting clay minerals (31). The later thermal-pulse model would imply that the ^{13}C-depleted cements were unrelated to the Marinoan meltdown. New tests are, therefore, needed to resolve this controversy. Here, we propose that if the precipitation of ^{13}C-depleted cements was, indeed, induced by MSR coupled to AOM early diagenetically, one would expect to observe—in addition to less than –30‰ $\delta^{13}C_{calc}$ (calcite cements or lenses)—at least four isotope data ranges and trends for the ^{13}C-depleted cements: 1) extremely negative $\delta^{13}C_{org}$ (organic carbon residues) values, down to as low as –68.7‰ as seen in modern seep carbonates because seep organisms inherit the ^{13}C-depleted carbon source from methane (32); 2) a wide range of $\delta^{34}S$ values for both carbonate-associated sulfate (CAS) and pyrite, due to Rayleigh-type isotope distillation in a closed to semiclosed void or crack settings; 3) a negative correlation between $\delta^{34}S$ and the small triple sulfur isotope deviation (i.e., the $\Delta^{33}S$) for both CAS and pyrite, a trend characteristic of cold-seep carbonate deposits due to an intrinsic triple sulfur isotope fractionation during MSR coupled to AOM (33); and 4) a positive correlation with a characteristic slope of less than 0.4 in $\delta^{18}O_{CAS}$-$\delta^{34}S_{CAS}$ space due to MSR in methane-seep environments (34, 35). Thus, in this study, we 1) extracted and measured the triple sulfur isotopes of pyrite and $\delta^{34}S$ and triple oxygen isotopes of CAS, as well as the $\delta^{13}C$ of the cements, host carbonates, and co-occurring organic residues in the ^{13}C-depleted cements; 2) estimated the likely range of marine $[SO_4]$ required for the precipitation of ^{13}C-depleted cements based on an existing model (36); and 3) constrained the timing of the deposition of the ^{13}C-depleted cements through $\delta^{13}C$ chemostratigraphic correlation of multiple sections to intervals bearing the earliest Ediacaran ^{17}O depletion episode in the Three Gorges–Shennongjia areas of South China.

Materials and Methods

The occurrences of the ^{13}C-depleted cements have been described in detail in previous studies (27–31). They are neither the usual pore water among fine grains nor open-water deposits, but instead chemical precipitates in restricted space such as voids and cracks of centimeter sizes in the host cap carbonates. These cements were collected from multiple field sections in South China (Fig. 1) and physically separated to minimize the mixing of the host dolostones using a rock saw. Multistep wet chemistry was applied to these samples. A few of the parameters are absent in some samples because the extracted CAS, pyrite, and/or organic residues were insufficient for analysis. Wet chemistry and stable isotope methods used in this study have been published in earlier works (37) and are outlined in *SI Appendix*. However, here, we combined carbon, oxygen, and sulfur isotope analyses including triple oxygen and triple sulfur isotope analyses for multiple compounds in a particular type of carbonate cement.

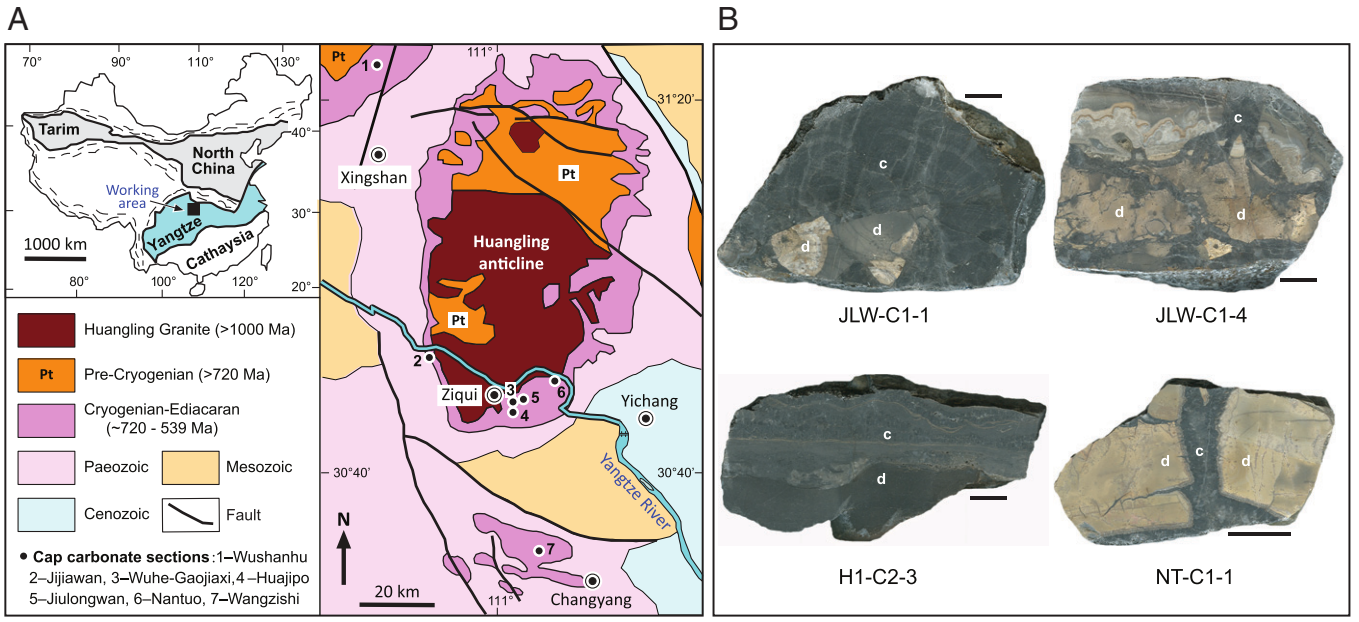

Fig. 1. (*A*) Simplified geological map showing location of sampled sections. (*B*) Examples of slabs of the ^{13}C-depleted cements from the basal Ediacaran cap carbonates. JLW-C1-1: ^{13}C-depleted cements coating the host dolostone breccias; JLW-C1-4: ^{13}C-depleted cements filling the cracks in host dolostones; H1-C2-3: layer-parallel, ^{13}C-depleted cements lenses within the host dolostone; NT-C1-1: ^{13}C-depleted cements cutting through the host dolostone. JLW-C1-1 and JLW-C1-4 are from the Jiulongwan (JLW) section (0.5 m and 0.7 m from the base of the cap carbonates, respectively); H1-C2-3 is from the Huajipo (HJP) section (2.4 m from the base of the cap carbonates); and NT-C1-1 is from the NT section (0.9 m from the base of the cap carbonated). c: ^{13}C-depleted cements; d: dolostone. (Scale bars, 1 cm.)

Results

The following data were acquired by this study. The $\delta^{13}C_{calc}$ values of the cements range from –44.3 to –4.0‰ Vienna Pee Dee Belemnite (VPDB). This range of $\delta^{13}C_{calc}$ values contrasts those of the host dolostones that range from –5.5 to 3.8‰ (VPDB) (Fig. 2*A*). The $\delta^{13}C$ values of the organic residues ($\delta^{13}C_{org}$) in cements range from –46.1 to –27.2‰, and they are lower than the $\delta^{13}C_{org}$ values of the hosting dolostones, which range from –31.7 to –26.5‰ (Fig. 2*A*). Additionally, the $\delta^{13}C_{org}$ and total organic carbon (TOC)% (ranging from 0 to 0.16 wt% of the bulk rock) were found to have a very weak (r^2 = 0.311) positive correlation (*SI Appendix*, Fig. S2). The $\delta^{34}S_{pyrite}$ values range from 22.8 to 73.9‰ Vienna Canyon Diablo Troilite in the cements and from 14.7 to 39.9‰ in the hosting dolostones (Fig. 2*B*). The $\delta^{34}S_{CAS}$ values range from 37.1 to 80.1‰ in the cements and from 24.5 to 41.5‰ in the hosting dolostones (Fig. 2*B*). The $\delta^{18}O_{CAS}$ values range from 12.9 to 22.2‰ Vienna Standard Mean Ocean Water in the cements and from 13.3 to 16.8‰ in the hosting dolostones (Fig. 2*C*). Additionally, the $\delta^{13}C_{org}$ and $\delta^{34}S_{pyrite}$ display a negative correlation (r^2 = 0.6; Fig. 2*B*), whereas the $\delta^{34}S_{CAS}$ and $\delta^{34}S_{pyrite}$ (r^2 = 0.9; Fig. 2*C*) and $\delta^{18}O_{CAS}$ and $\delta^{34}S_{CAS}$ plots (r^2 = 0.9; Fig. 2*D*) display strong positive correlations for the cements. Furthermore, the $\Delta^{33}S_{pyrite}$ [defined as $\Delta^{33}S = \delta^{33}S - 1000([1 + \delta^{34}S/1000]^{0.515} - 1)$] vary from –0.064 to 0.057‰ and are negatively correlated with the corresponding $\delta^{34}S_{pyrite}$ values for the cements (r^2 = 0.5, Fig. 2*E*).

Discussion

The Origin of ^{13}C-Depleted Cements. Multiple isotope data of various compounds (i.e., host dolostones, calcite cements and lenses, pyrite, CAS, and organic residues), as well as geological occurrence, support an origin of sulfate reduction coupled to AOM in cold-seep settings for the ^{13}C-depleted cements. As previously suggested (38), $\delta^{13}C_{carb}$ values lower than −30‰ (Fig. 2*A*) can serve as a "litmus test" for methane-derived carbon. However, low $\delta^{13}C_{carb}$ values alone cannot distinguish sulfate reduction from biological (e.g., refs. 39, 40) or abiological (41) Fe(III)- or Mn (IV)-reduction coupled to AOM. Carbonates formed via both sulfate- and Fe- or Mn-reduction paths can have $\delta^{13}C_{carb}$ values as negative as –70‰ (41). However, both biological and abiological Fe (III)- or Mn (IV)-reduction coupled to AOM would have incorporated large amounts of Fe and Mn into precipitated calcite cements. The reported Fe contents in the ^{13}C-depleted cements are ∼10 times lower than host dolostones, whereas the Mn contents are similar to or slightly higher than those in the host dolostones of the basal Doushantuo Formation (3, 31), thus negating the possibility of Fe(III)-reduction but leaving open the possibility of Mn(IV)-reduction before sulfate reduction coupled to AOM. Additionally, if microbial activities were closely involved in the precipitation of the ^{13}C-depleted cements, the calcite would have extremely ^{13}C-depleted organic matter incorporated as well, due to seep biomass contributions from a consortium of archaea and sulfate-reducing bacteria (42). This inference is confirmed by $\delta^{13}C_{org}$ values ranging from −29 to −68‰ in modern cold-seep carbonates from the Gulf of Mexico (32). The low $\delta^{13}C_{org}$ values, down to −46.1‰ measured here, in the ^{13}C-depleted cements (Fig. 2*A*) support a cold-seep origin. In addition, the weakly positive correlation between $\delta^{13}C_{org}$ and TOC% is consistent with a mixing of organic matter between seawater and seep environments.

Positive $\delta^{18}O_{CAS}$– $\delta^{34}S_{CAS}$ and $\delta^{34}S_{CAS}$– $\delta^{34}S_{pyrite}$ correlations reveal active MSR during the precipitation of the ^{13}C-depleted cements. MSR produces ^{34}S-depleted sulfides and results in the precipitation of pyrite that has $\delta^{34}S$ values 4 to 70‰ lower than its starting sulfate (43, 44). In methane-rich environments, progressive sulfate reduction may lead to sulfate depletion in a restricted water mass, potentially resulting in elevated $\delta^{34}S$ values for both sulfate and pyrite due to isotope

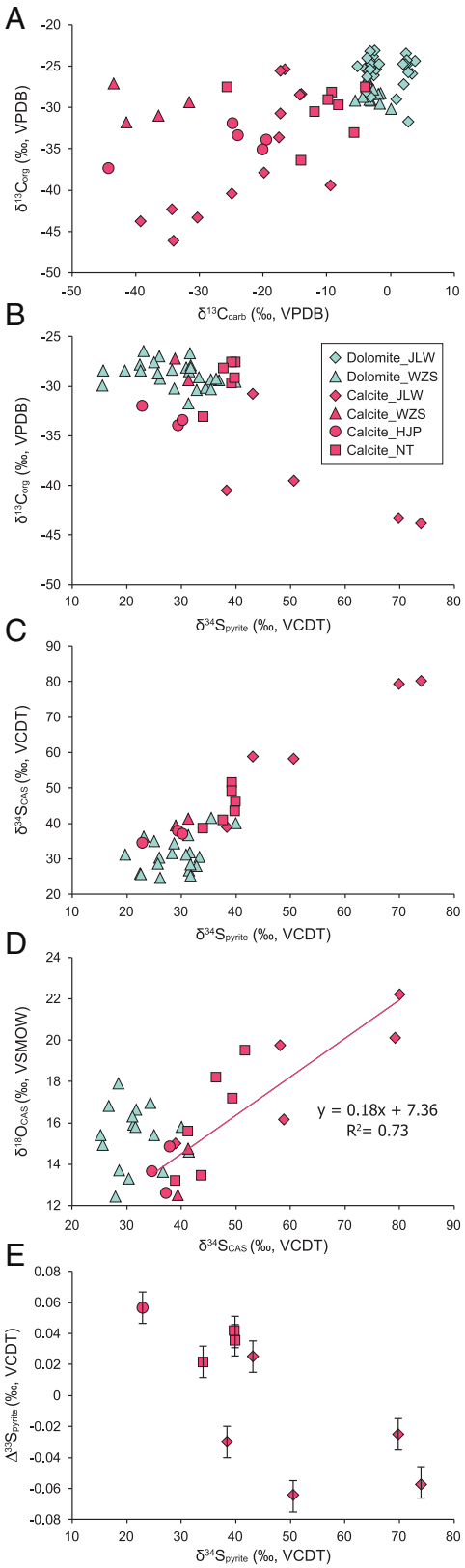

Fig. 2. Cross plots of $\delta^{13}C_{carb}$–$\delta^{13}C_{org}$ (*A*), $\delta^{13}C_{org}$–$\delta^{34}S_{pyrite}$ (*B*), $\delta^{34}S_{CAS}$–$\delta^{34}S_{pyrite}$ (*C*), $\delta^{18}O_{CAS}$–$\delta^{34}S_{CAS}$ (*D*), and $\Delta^{33}S_{pyrite}$–$\delta^{34}S_{pyrite}$ (*E*) of the ^{13}C-depleted cements and their hosting dolostones from the basal Doushantuo Formation member around the Three Gorge area, South China. Sections: JLW, Wangzishi (WZS), NT, HJP. Analytical uncertainties are smaller than the sizes of the symbols except where plotted.

fractionation in a limited reservoir. As a result, seep carbonates commonly have highly variable $\delta^{34}S_{CAS}$ and $\delta^{34}S_{pyrite}$ values that often positively correlate (34). Variable $\delta^{34}S_{CAS}$ (37.1 to 80.1‰) and $\delta^{34}S_{pyrite}$ (22.8 to 73.9‰) values and their positive correlation for the ^{13}C-depleted cements (Fig. 2*C*) are consistent with progressive sulfate reduction coupled to AOM in a methane-rich but flow-restricted environment. The positive $\delta^{18}O_{CAS}$–$\delta^{34}S_{CAS}$ correlation with a slope of 0.18 for the ^{13}C-depleted cements (Fig. 2*D*) suggests high sulfate reduction rates that are diagnostic of MSR coupled to AOM, and the correlation has an identical trend to those observed in modern and ancient cold-seep carbonates (34, 35).

Negative $\delta^{13}C_{org}$ – $\delta^{34}S_{pyrite}$ (Fig. 2*B*) and $\Delta^{33}S_{pyrite}$–$\delta^{34}S_{pyrite}$ (Fig. 2*E*) correlations provide additional support for a cold-seep origin of the ^{13}C-depleted cements. High $\delta^{34}S_{pyrite}$ and low $\delta^{13}C_{org}$ values suggest that in methane-rich waters, sulfate-depleted conditions with limited sulfate replenishment also favor the preservation of organic matter sourced from seep organisms. A distinctly negative $\Delta^{33}S$–$\delta^{34}S$ correlation has been observed for barites in modern cold-seep carbonates, which has been attributed to MSR coupled to AOM having a characteristic triple sulfur isotope relationship (i.e., a lower $^{33}\theta$ ($^{33}\theta \equiv \ln^{33}\alpha/\ln^{34}\alpha$) value than that of typical organotrophic sulfate reduction processes; ref. 33). The sizable ranges of $\Delta^{33}S_{pyrite}$ for mass-dependent processes and $\delta^{34}S_{pyrite}$ observed in the ^{13}C-depleted cements are also consistent with pyrite being the product of MSR coupled to AOM (45). Thermochemically generated pyrite, however, would not have highly variable $\delta^{34}S_{pyrite}$ (range up to 60‰) or values up to +74‰, nor would it display a range of 0.12‰ in $\Delta^{33}S_{pyrite}$ values (46). In summary, the highly variable $\delta^{13}C_{org}$, $\delta^{34}S_{CAS}$, $\delta^{34}S_{pyrite}$, $\delta^{18}O_{CAS}$, and $\Delta^{33}S_{pyrite}$ values and their correlations all support an early diagenetic cold-seep origin of the ^{13}C-depleted cements in the basal Ediacaran in South China.

Constraining Earliest Ediacaran Marine Sulfate Evolution. The cold-seep origin of the ^{13}C-depleted cements places a constraint on the minimum [SO_4] in ambient waters at the time of their deposition. Bristow and Grotzinger (36) constructed a one-dimensional, carbon-isotope-enabled reaction-transport model to explore pore water ion chemistry in sediment by considering diffusion, advection, and chemical reactions—in particular, different rates of AOM. In their model sensitivity tests, [DIC], [SO_4], and the carbon isotope composition of methane are the three dominant parameters found to influence the mean $\delta^{13}C$ of carbonates in pore waters. To calculate the [SO_4] required to generate ^{13}C-depleted cements with a $\delta^{13}C_{carb}$ value at –48‰, we need to constrain the other two variables. If we accept that the mean $\delta^{13}C$ value of marine basin methane is at –65‰ and the marine [DIC] in the earliest Ediacaran was 4 times that of the modern ocean (47), Bristow and Grotzinger's model would require ~30 mM [SO_4] according to their fig. 2. This [SO_4] estimate is sensitive to the average $\delta^{13}C$ value of methane used in the simulation with a higher value requiring higher ambient [SO_4]. The –65‰ of methane is the value used in the Bristow and Grotzinger model and is roughly the mean of the methane $\delta^{13}C$ values in modern ocean basins (e.g., ref. 48), and there is no compelling reason why this mean value would be different in the early Ediacaran. Marine [DIC] in the late Precambrian is poorly constrained, but models based on evidence such as microbial calcification and pCO_2 all point to much higher [DIC] (49, 50). Some modeling studies assumed much higher [DIC] (e.g., as high as 36 times the present value for the Precambrian; refs. 51, 52). A higher [DIC] would also require greater [SO_4] to explain the observed $\delta^{13}C_{carb}$ value of –48‰; thus, our estimate of 30 mM [SO_4] may be an underestimate. Regardless, even the 30 mM [SO_4] is several times higher than the previous average [SO_4] estimates of <5 mM for much of

the Mesoproterozoic (53) and 0.3 to 3 mM for the very early Ediacaran ocean (17). On the other hand, if the ^{13}C-depleted cements precipitated largely in the meltwater lid, the DIC concentration there could be much lower or higher depending on the alkalinity of the water (54). We argue that a high [DIC] water for the cements is still most likely because 1) high pH river water is expected during the intense postpanglacial weathering, and 2) the anoxic condition for the cement precipitation favors a significant portion of bottom water that was high in [DIC]. Further modeling studies can explore the role of meltwater lid in the precipitation of the ^{13}C-depleted cements.

Similar ^{13}C-depleted cements are not common in other members of the Doushantuo Formation, except for their sporadic presence in the upper Doushantuo Formation with $\delta^{13}C_{carb}$ as low as –34‰ (55–57). This could mean either that high regional concentrations of marine sulfate did not last long, or, similarly, that ^{13}C-depleted seep carbonates were not deposited or have not been found yet. Moreover, [SO_4] may have been spatially heterogeneous, with high concentrations near shore and low concentrations in the open ocean or at depth. While sulfate levels likely fell after this transient peak, low $\delta^{34}S_{pyrite}$ values in black shales (member II) overlying the basal carbonates (member I) (58) suggest that they were subsequently maintained at higher levels than the Proterozoic background (59). If this model is correct, marine [SO_4] also likely peaked during a transient episode associated with the Shuram Excursion if one considers the sporadic occurrence of ^{13}C-depleted cements in this part of the upper Doushantuo Formation, which is consistent with the occurrence of barite and other sulfate minerals in the sediments of this interval (60). We note that the basal Ediacaran ^{13}C-depleted cements are the earliest known case of carbonates derived from MSR coupled to AOM. There is no report of similarly ^{13}C-depleted carbonate deposits in the postglacial sediments of the Sturtian or Paleoproterozoic panglaciations. Furthermore, it is not until the late Devonian that ^{13}C-depleted cements have been identified in the sedimentary record (37). The potential for preservation bias notwithstanding, our findings suggest that although both a high methane flux and high [SO_4] are necessary conditions for the deposition of ^{13}C-depleted cements, high marine [SO_4] rivaling modern levels may have only re-emerged in the Devonian. In the particular case of the earliest Ediacaran period, high fluxes of methane encountered an episode of high [SO_4] sometime after the marine transgression that inundated basal Ediacaran cap dolostones in South China (27).

Time Constraints. The stratigraphic confinement of the dark-colored, ^{13}C-depleted cements within the basal member of the Doushantuo Formation rules out a later diagenetic origin. Had a thermal pulse acted on these buried stratigraphic sequences later in the Ediacaran, or even in the Cambrian (31), we would have seen similarly dark-colored ^{13}C-depleted cements throughout the late Ediacaran or even up to the Cambrian deposits in South China. A late diagenetic origin for the ^{13}C-depleted cements is also unlikely because of the need for DIC sourced from MSR coupled to AOM, for which access to marine sulfate is required.

To further constrain and correlate the interval of the ^{13}C-depleted cements, we turn to regional $\delta^{13}C_{carb}$ chemostratigraphy in the Three Gorge–Shennongjia areas. We note that while the expression of geochemical variations can vary due to local processes, and diagenetic processes can significantly decouple local records from global marine signatures (e.g., ref. 61), the regionally correlated positive $\delta^{13}C_{carb}$ shift of 4 to 8‰ is most readily explained through contemporaneous shifts in carbon cycling across the Three Gorge–Shennongjia areas (Fig. 3). The ^{13}C-depleted cements in the four shallow-water sections all occur before the positive $\delta^{13}C_{carb}$ shift, with some possibly extending into the beginning of the positive $\delta^{13}C_{carb}$ shift. In addition, Killingsworth et al. (10) reported 11 barite layers in a near-shore and condensed section of the basal Doushantuo Formation at Wushanhu, Shennongjia, ~200 km northwest of the Three Gorge area, and constrained the maximum duration of the earliest Ediacaran ^{17}O depletion episode to be <1 My based on a combination of chemostratigraphic correlation and existing geochronological constraints. In Wushanhu, we see the earliest Ediacaran ^{17}O depletion episode encompasses an extended stretch of the positive $\delta^{13}C_{carb}$ shift and, thus, conclude from the chemostratigraphic correlation that the positive $\delta^{13}C_{carb}$ shift occurred within the same time window as the earliest Ediacaran ^{17}O depletion episode. Therefore, the ^{13}C-depleted cements were deposited during the earliest Ediacaran ^{17}O depletion episode in the Three Gorge–Shennongjia areas (Figs. 1 and 3). The significantly negative $\Delta^{17}O_{SO4}$ range, which defines the earliest Ediacaran ^{17}O depletion episode, suggests atmospheric pO_2 and pCO_2 of similar magnitude across this interval (16). Therefore, the temporal overlap between ^{13}C-depleted cements and the basal Ediacaran ^{17}O depletion interval may not be coincidental. The overlap occurred at a time when decreasing pCO_2 and rising pO_2 were at optimum levels amenable to generate the necessary combination of oxidative weathering and sulfide burial fluxes to achieve a transient maximum in early Ediacaran marine [SO_4], at least in the shallow seas of South China.

The timing of the earliest Ediacaran ^{17}O depletion episode is closely linked to the postmeltdown Earth's surface dynamics, which can provide critical information on the rates of change of the early Ediacaran biosphere and atmosphere. As noted above, current radiometric dates (Fig. 3) constrain the duration of the earliest Ediacaran ^{17}O depletion episode to be within 1 My (10, 62). Additional radiometric dates would help, but they are limited to the availability of volcanic materials as well as dating resolution (i.e., 10^5 y or an even shorter time resolution is needed [see below] for materials of ~635 Ma, which is not analytically possible at this time). Global biogeochemical modeling also places the earliest Ediacaran ^{17}O depletion episode to be within 1 My (16). An effort to interpret observed relative sea-level changes on the South China continental shelf through a glacial isostatic adjustment model places an independent constraint on the earliest Ediacaran ^{17}O depletion episode at ~10^5 y (63).

Another absolute time constraint comes from the global energetic constraints, which place a best estimate of ~5×10^4 y for the postdeglaciation meltwater lid (11). Indeed, if layers of sedimentary barite crystal fans in the postmeltdown successions of the basal Ediacaran are the result of episodic disruptions of the chemically stratified ocean—as is consistent with a deep-water supply of Ba^{2+} in current barite formation models (8, 9, 17, 64)—the disappearance of these barite layers should mark a complete destratification or the end of the meltwater lid. Thus, data from Wushanhu in South China, where many ^{17}O-anomalous barite layers are overlain by at least four ^{17}O-normal barite layers, should place the duration of the earliest Ediacaran ^{17}O depletion episode to be within less than 5×10^4 y. That is, both the earliest Ediacaran ^{17}O depletion and the peak marine sulfate episodes ended before the meltwater lid or the dynamically stratified ocean did. Therefore, the ^{13}C-depleted cements in South China were likely deposited when [SO_4] in the meltwater lid was at or above modern levels for a brief

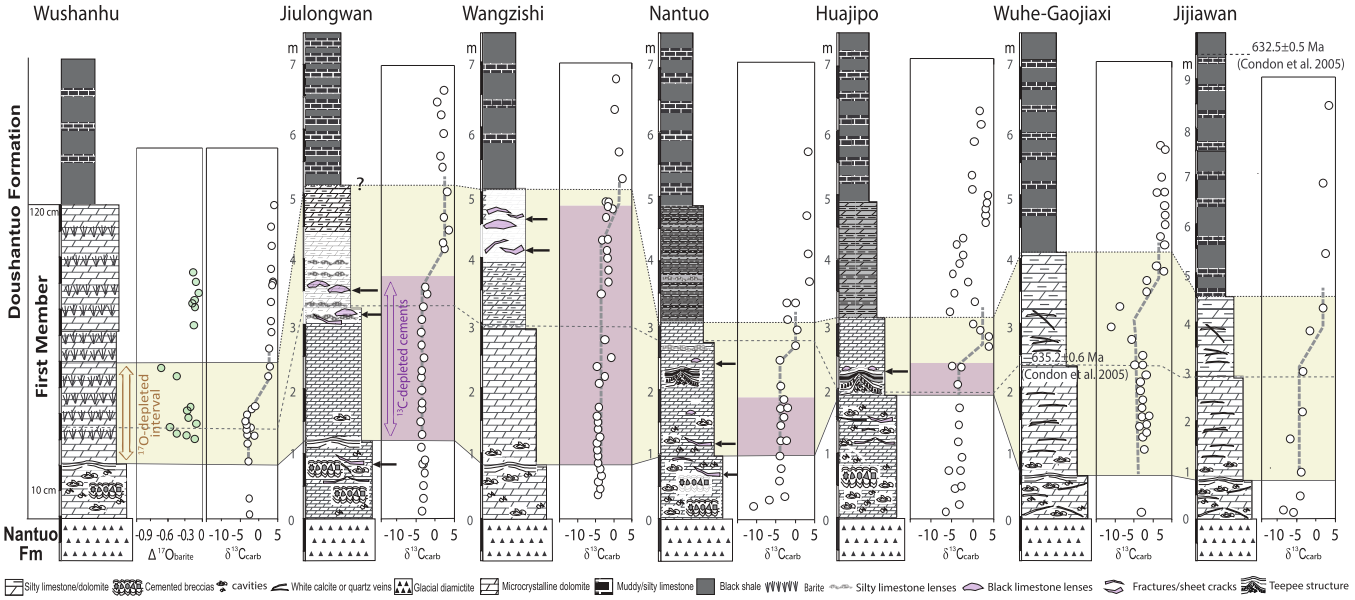

Fig. 3. Lithostratigraphy; carbon isotope chemostratigraphy; stratigraphic occurrence of the basal Ediacaran ^{17}O-depletion interval and ^{13}C-depleted cements (marked with black arrows); and correlation of radiometric ages for seven shallow-platform basal Ediacaran sections in the Three Gorges–Shennongjia area, South China. The yellow-shaded intervals are inferred to be the earliest Ediacaran ^{17}O depletion episodes based on the relationship between a regional $\delta^{13}C$ positive shift and a known basal Ediacaran ^{17}O depletion interval at Wushanhu. The Wushanhu section has a dozen or so barite layers occurring in the basal Ediacaran carbonates, representing probably the shallowest section in the region. The cranberry-colored intervals are where the ^{13}C-depleted cements occur in the four listed sections based on field and isotope data. Note that we interpret that the void-filling ^{13}C-depleted cements in the basal cap dolostones were formed after the deposition of the host dolostones. Two U-Pb dates from Jijiawan and Wuhe-Gaojiaxi are from Condon et al. (66). A U-Pb date of 634.57 ± 0.88 Ma was obtained at the topmost NT diamictite in the Eshan/Tiechang section in Yunnan Province (62). Carbon isotope data of the Wushanhu section are from Killingsworth et al. (10), the Jijiawan section from Zhang et al. (67), the Wuhe-Gaojiaxi section from Sawaki et al. (68), and the JLW and WZS sections from Wang et al. (29). Black arrows mark our sample positions.

duration when atmospheric CO_2 and O_2 concentrations were of a similar magnitude (16), and both events occurred in less than 5×10^4 y after the onset of deglaciation.

Bristow et al. (31) and this study share the same conclusion that methane oxidation–derived carbon was responsible for the ^{13}C-depleted cements. Conclusions diverge, however, regarding the methane source: Bristow et al. (31) suggest thermogenic methane oxidation at depth, whereas our results suggest microbial methane oxidation in shallow sediments. The former model (31) suggests a local, short-lived thermal event (>300 °C) occurring at least 1.6 My after deposition of the cap carbonates, while the latter advocates for shallow and early diagenetic precipitation in the upper part of the cap carbonates and within 5×10^4 y after the onset of the deglaciation.

If our conclusions stand, the rate of biosphere–atmospheric transformation in the immediate post-snowball world is astonishing. Whereas the earliest Ediacaran ^{17}O depletion episode must have been global because it was an atmospheric event (15, 18, 65), a rapid rise of marine $[SO_4]$, to the degree that we have assessed here, was likely regional because the two major controlling factors (i.e., oxidative weathering on the continents and pyrite burial in marine sediments) are regional at the 10^4 to 10^5 y timescales. While these arguments can explain why ^{13}C-depleted cements have, thus far, been reported only in the earliest Ediacaran in South China, it is likely that continued investigation of basal Ediacaran sequences will expand their occurrence. Such an expansion may add yet another globally diagnostic phenomena of enigmatic post-Marinoan sediments.

Data Availability. All relevant data to this study are included in the article and/or *SI Appendix*.

ACKNOWLEDGMENTS. Financial support is provided by National Natural Science Foundation of China Grant 42173001 to Y.P., Nanjing University, and NSF (EAR-2021207) to S.X. P.C. acknowledges funding from the Zuckerman STEM Leadership program and The Natural Sciences and Engineering Research Council of Canada.

Author affiliations: [a]International Center for Isotope Effects Research, Nanjing University, Nanjing 210023, China; [b]School of Earth Sciences and Engineering, Nanjing University, Nanjing 210023, China; [c]Department of Geoscience, University of Nevada, Las Vegas, NV 89154; [d]Department of Earth and Planetary Science, Harvard University, Cambridge, MA 02138; [e]Department of Earth and Planetary Sciences, Weizmann Institute of Science, Rehovot 7610001, Israel; [f]Shanghai Engineering Research Center of Hadal Science and Technology, College of Marine Sciences, Shanghai Ocean University, Shanghai 201306, China; [g]Department of Geosciences, Virginia Tech, Blacksburg, VA 24061; [h]Department of Geology, University of Maryland, College Park, MD 20742; [i]State Key Laboratory of Biogeology and Environment Geology, China University of Geosciences, Wuhan 430074, China; and [j]Hubei Key Laboratory of Marine Geological Resources, China University of Geosciences, Wuhan 430074, China

1. J. Li *et al.*, Continental weathering intensity during the termination of the Marinoan Snowball Earth: Mg isotope evidence from the basal Doushantuo cap carbonate in South China. *Palaeogeogr. Palaeoclimatol. Palaeoecol.* **552**, 109774 (2020).
2. X. Yang, X. Long, J. Li, Y. Dong, B. Zhao, Mo isotopic response to the end of Neoproterozoic Marinoan glaciation: Evidence from a sedimentary profile in South China. *Precambrian Res.* **339**, 105609 (2020).
3. K.-J. Huang *et al.*, Episode of intense chemical weathering during the termination of the 635 Ma Marinoan glaciation. *Proc. Natl. Acad. Sci. U.S.A.* **113**, 14904–14909 (2016).
4. X. Lang *et al.*, Transient marine euxinia at the end of the terminal Cryogenian glaciation. *Nat. Commun.* **9**, 3019 (2018).
5. G. Le Hir, Y. Goddéris, Y. Donnadieu, G. Ramstein, A geochemical modelling study of the evolution of the chemical composition of seawater linked to a "snowball" glaciation. *Biogeosciences* **5**, 253–267 (2008).
6. M. Kunzmann *et al.*, Zn isotope evidence for immediate resumption of primary productivity after snowball Earth. *Geology* **41**, 27–30 (2013).
7. P. F. Hoffman *et al.*, Snowball Earth climate dynamics and Cryogenian geology-geobiology. *Sci. Adv.* **3**, e1600983 (2017).
8. Y. B. Peng, H. Bao, C. M. Zhou, X. L. Yuan, ^{17}O-depleted barite from two Marinoan cap dolostone sections, South China. *Earth Planet. Sci. Lett.* **305**, 21–31 (2011).
9. P. W. Crockford *et al.*, Barium-isotopic constraints on the origin of post-Marinoan barites. *Earth Planet. Sci. Lett.* **519**, 234–244 (2019).
10. B. A. Killingsworth, J. A. Hayles, C. Zhou, H. Bao, Sedimentary constraints on the duration of the Marinoan Oxygen-17 Depletion (MOSD) event. *Proc. Natl. Acad. Sci. U.S.A.* **110**, 17686–17690 (2013).
11. J. Yang, M. F. Jansen, F. A. Macdonald, D. S. Abbot, Persistence of a freshwater surface ocean after a snowball Earth. *Geology* **45**, 615–618 (2017).

12. A. S. C. Ahm *et al.*, An early diagenetic deglacial origin for basal Ediacaran "cap dolostones". *Earth Planet. Sci. Lett.* **506**, 292–307 (2019).
13. M. Kunzmann *et al.*, Bacterial sulfur disproportionation constrains timing of Neoproterozoic oxygenation. *Geology* **45**, 207–210 (2017).
14. H. Bao, I. J. Fairchild, P. M. Wynn, C. Spötl, Stretching the envelope of past surface environments: Neoproterozoic glacial lakes from Svalbard. *Science* **323**, 119–122 (2009).
15. H. Bao, J. R. Lyons, C. Zhou, Triple oxygen isotope evidence for elevated CO_2 levels after a Neoproterozoic glaciation. *Nature* **453**, 504–506 (2008).
16. X. Cao, H. Bao, Dynamic model constraints on oxygen-17 depletion in atmospheric O_2 after a snowball Earth. *Proc. Natl. Acad. Sci. U.S.A.* **110**, 14546–14550 (2013).
17. P. W. Crockford *et al.*, Triple oxygen and multiple sulfur isotope constraints on the evolution of the post-Marinoan sulfur cycle. *Earth Planet. Sci. Lett.* **435**, 74–83 (2016).
18. P. W. Crockford *et al.*, Linking paleocontinents through triple oxygen isotope anomalies. *Geology* **46**, 179–182 (2018).
19. K. A. McFadden *et al.*, Pulsed oxidation and biological evolution in the Ediacaran Doushantuo Formation. *Proc. Natl. Acad. Sci. U.S.A.* **105**, 3197–3202 (2008).
20. Q. Ouyang *et al.*, Distribution of Ediacaran acanthomorphic acritarchs in the lower Doushantuo Formation of the Yangtze Gorges area, South China: Evolutionary and stratigraphic implications. *Precambrian Res.* **353**, 106005 (2021).
21. W. Yao, A. Paytan, U. G. Wortmann, Large-scale ocean deoxygenation during the Paleocene-Eocene Thermal Maximum. *Science* **361**, 804–806 (2018).
22. W. Q. Yao, A. Paytan, U. G. Wortmann, Effects of a transient marine sulfur reservoir on seawater δ^{18}O(SO4) during the Paleocene-Eocene Thermal Maximum. *Geochim. Cosmochim. Acta* **269**, 257–269 (2020).
23. A. C. Johnson *et al.*, Experimental determination of pyrite and molybdenite oxidation kinetics at nanomolar oxygen concentrations. *Geochim. Cosmochim. Acta* **249**, 160–172 (2019).
24. S. Fabre, G. Berger, How tillite weathering during the snowball Earth aftermath induced cap carbonate deposition. *Geology* **40**, 1027–1030 (2012).
25. S. G. John, M. Kunzmann, E. J. Townsend, A. D. Rosenberg, Zinc and cadmium stable isotopes in the geological record: A case study from the post-snowball Earth Nuccaleena cap dolostone. *Palaeogeogr. Palaeoclimatol. Palaeoecol.* **466**, 202–208 (2017).
26. G. Q. Jiang, M. J. Kennedy, N. Christie-Blick, H. C. Wu, S. H. Zhang, Stratigraphy, sedimentary structures, and textures of the late Neoproterozoic Doushantuo cap carbonate in South China. *J. Sediment. Res.* **76**, 978–995 (2006).
27. C. Zhou, H. Bao, Y. Peng, X. Yuan, Timing the deposition of ^{17}O-depleted barite at the aftermath of Nantuo glacial meltdown in South China. *Geology* **38**, 903–906 (2010).
28. C. M. Zhou, C. G. Guan, H. Cui, Q. Ouyang, W. Wang, Methane-derived authigenic carbonate from the lower Doushantuo Formation of South China: Implications for seawater sulfate concentration and global carbon cycle in the early Ediacaran ocean. *Palaeogeogr. Palaeoclimatol. Palaeoecol.* **461**, 145–155 (2016).
29. J. S. Wang, G. Q. Jiang, S. H. Xiao, Q. Li, Q. Wei, Carbon isotope evidence for widespread methane seeps in the ca. 635 Ma Doushantuo cap carbonate in south China. *Geology* **36**, 347–350 (2008).
30. G. Jiang, M. J. Kennedy, N. Christie-Blick, Stable isotopic evidence for methane seeps in Neoproterozoic postglacial cap carbonates. *Nature* **426**, 822–826 (2003).
31. T. F. Bristow, M. Bonifacie, A. Derkowski, J. M. Eiler, J. P. Grotzinger, A hydrothermal origin for isotopically anomalous cap dolostone cements from south China. *Nature* **474**, 68–71 (2011).
32. Y. Sun *et al.*, A new approach to discern the hydrocarbon sources (oil vs. methane) of authigenic carbonates forming at marine seeps. *Mar. Pet. Geol.* **114**, 104230 (2020).
33. S. G. Gong *et al.*, Triple sulfur isotope relationships during sulfate-driven anaerobic oxidation of methane. *Earth Planet. Sci. Lett.* **504**, 13–20 (2018).
34. D. Feng *et al.*, A carbonate-based proxy for sulfate-driven anaerobic oxidation of methane. *Geology* **44**, 999–1002 (2016).
35. G. Antler, A. V. Turchyn, B. Herut, O. Sivan, A unique isotopic fingerprint of sulfate-driven anaerobic oxidation of methane. *Geology* **43**, 619–622 (2015).
36. T. F. Bristow, J. P. Grotzinger, Sulfate availability and the geological record of cold-seep deposits. *Geology* **41**, 811–814 (2013).
37. Y. Peng *et al.*, Widespread contamination of carbonate-associated sulfate by present-day secondary atmospheric sulfate: Evidence from triple oxygen isotopes. *Geology* **42**, 815–818 (2014).
38. K. A. Campbell, Hydrocarbon seep and hydrothermal vent paleoenvironments and paleontology: Past developments and future research directions. *Palaeogeogr. Palaeoclimatol. Palaeoecol.* **232**, 362–407 (2006).
39. K. F. Ettwig *et al.*, Archaea catalyze iron-dependent anaerobic oxidation of methane. *Proc. Natl. Acad. Sci. U.S.A.* **113**, 12792–12796 (2016).
40. E. J. Beal, C. H. House, V. J. Orphan, Manganese- and iron-dependent marine methane oxidation. *Science* **325**, 184–187 (2009).
41. W.-X. Hu *et al.*, Thermochemical oxidation of methane induced by high-valence metal oxides in a sedimentary basin. *Nat. Commun.* **9**, 5131 (2018).
42. A. Boetius *et al.*, A marine microbial consortium apparently mediating anaerobic oxidation of methane. *Nature* **407**, 623–626 (2000).
43. M. S. Sim, T. Bosak, S. Ono, Large sulfur isotope fractionation does not require disproportionation. *Science* **333**, 74–77 (2011).
44. B. A. Wing, I. Halevy, Intracellular metabolite levels shape sulfur isotope fractionation during microbial sulfate respiration. *Proc. Natl. Acad. Sci. U.S.A.* **111**, 18116–18125 (2014).
45. A. Crémière, A. Pellerin, B. A. Wing, A. Lepland, Multiple sulfur isotopes in methane seep carbonates track unsteady sulfur cycling during anaerobic methane oxidation. *Earth Planet. Sci. Lett.* **532**, 115994 (2020).
46. J. Labidi, P. Cartigny, C. Hamelin, M. Moreira, L. Dosso, Sulfur isotope budget (^{32}S, ^{33}S, ^{34}S and ^{36}S) in Pacific–Antarctic ridge basalts: A record of mantle source heterogeneity and hydrothermal sulfide assimilation. *Geochim. Cosmochim. Acta* **133**, 47–67 (2014).
47. A. Ridgwell, A Mid Mesozoic Revolution in the regulation of ocean chemistry. *Mar. Geol.* **217**, 339–357 (2005).
48. J. D. Kessler *et al.*, A survey of methane isotope abundance (14C, 13C, 2H) from five nearshore marine basins that reveals unusual radiocarbon levels in subsurface waters. *J. Geophys. Res. Oceans* **113**, C12021 (2008).
49. G. Arp, A. Reimer, J. Reitner, Photosynthesis-induced biofilm calcification and calcium concentrations in Phanerozoic oceans. *Science* **292**, 1701–1704 (2001).
50. J. K. Bartley, L. C. Kah, Marine carbon reservoir, Corg-Ccarb coupling, and the evolution of the Proterozoic carbon cycle. *Geology* **32**, 129–132 (2004).
51. T. Bosak, D. K. Newman, Microbial nucleation of calcium carbonate in the Precambrian. *Geology* **31**, 577–580 (2003).
52. I. Halevy, M. Alesker, E. M. Schuster, R. Popovitz-Biro, Y. Feldman, A key role for green rust in the Precambrian oceans and the genesis of iron formations. *Nat. Geosci.* **10**, 135–139 (2017).
53. L. C. Kah, T. W. Lyons, T. D. Frank, Low marine sulphate and protracted oxygenation of the Proterozoic biosphere. *Nature* **431**, 834–838 (2004).
54. J. J. Cole, Y. T. Prairie, "Dissolved CO_2 in freshwater systems" in *Reference Module in Earth Systems and Environmental Sciences* (Elsevier, 2014).
55. H. Cui *et al.*, Phosphogenesis associated with the Shuram Excursion: Petrographic and geochemical observations from the Ediacaran Doushantuo Formation of South China. *Sediment. Geol.* **341**, 134–146 (2016).
56. S. Furuyama, A. Kano, Y. Kunimitsu, T. Ishikawa, W. Wang, Diagenetic overprint to a negative carbon isotope anomaly associated with the Gaskiers glaciation of the Ediacaran Doushantuo Formation in South China. *Precambrian Res.* **276**, 110–122 (2016).
57. M. Macouin *et al.*, Combined paleomagnetic and isotopic data from the Doushantuo carbonates, South China: Implications for the "snowball Earth" hypothesis. *Earth Planet. Sci. Lett.* **224**, 387–398 (2004).
58. S. K. Sahoo *et al.*, Ocean oxygenation in the wake of the Marinoan glaciation. *Nature* **489**, 546–549 (2012).
59. G. P. Halverson, M. T. Hurtgen, Ediacaran growth of the marine sulfate reservoir. *Earth Planet. Sci. Lett.* **263**, 32–44 (2007).
60. H. Cui *et al.*, Dynamic interplay of biogeochemical C, S and Ba cycles in response to the Shuram oxygenation event. *J. Geol. Soc. London* **179**, jgs2021-081 (2021).
61. P. W. Crockford *et al.*, Reconstructing Neoproterozoic seawater chemistry from early diagenetic dolomite. *Geology* **49**, 442–446 (2021).
62. C. Zhou, M. H. Huyskens, X. Lang, S. Xiao, Q.-Z. Yin, Calibrating the terminations of Cryogenian global glaciations. *Geology* **47**, 251–254 (2019).
63. Y. Irie, M. Nakada, J. Okuno, H. M. Bao, Nonmonotonic postdeglacial relative sea level changes at the Aftermath of Marinoan (635 Ma) Snowball Earth Meltdown. *J. Geophys. Res. Solid Earth* **124**, 9373–9394 (2019).
64. G. A. Shields, M. Deynoux, H. Strauss, H. Paquet, D. Nahon, Barite-bearing cap dolostones of the Taoudeni Basin, northwest Africa: Sedimentary and isotopic evidence for methane seepage after a Neoproterozoic glaciation. *Precambrian Res.* **153**, 209–235 (2007).
65. H. Bao, Z.-Q. Chen, C. Zhou, An ^{17}O record of late Neoproterozoic glaciation in the Kimberley region, Western Australia. *Precambrian Res.* **216–219**, 152–161 (2012).
66. D. Condon *et al.*, U-Pb ages from the neoproterozoic Doushantuo Formation, China. *Science* **308**, 95–98 (2005).
67. S. H. Zhang *et al.*, U-Pb sensitive high-resolution ion microprobe ages from the Doushantuo Formation in south China: Constraints on late Neoproterozoic glaciations. *Geology* **33**, 473–476 (2005).
68. Y. Sawaki *et al.*, The Ediacaran radiogenic Sr isotope excursion in the Doushantuo Formation in the Three Gorges area, South China. *Precambrian Res.* **176**, 46–64 (2010).